

Estimations of Regional Surface Energy Fluxes Over Heterogeneous Oasis–Desert Surfaces in the Middle Reaches of the Heihe River During HiWATER-MUSOEXE

Yanfei Ma, Shaomin Liu, Fen Zhang, Ji Zhou, Zhenzhen Jia, and Lisheng Song

Abstract—The determination of the spatial heterogeneity of the regional evapotranspiration over a complex underlying surface in an oasis–desert region is crucial for water resource management in a river basin and aiding in irrigation decisions. The surface energy balance system (SEBS) model has been widely used to estimate surface energy fluxes. However, the parameterization of surface roughness length for momentum transfer (z_{0m}) and heat transfer (z_{0h}) did not perform well for a complex underlying surface. Moreover, it is difficult to estimate surface soil heat flux, i.e., G_0 , accurately at the regional scale. In this letter, the parameterization schemes of z_{0m} , z_{0h} , and G_0 were optimized. Measurements from 21 sets of eddy covariance systems were used to validate the model performance. The results show that the revised SEBS model root-mean-square errors (RMSEs) of the satellite-based sensible and latent heat fluxes (H and LE) decreased from $97.2 \text{ W} \cdot \text{m}^{-2}$ to $56.9 \text{ W} \cdot \text{m}^{-2}$ and from $102.9 \text{ W} \cdot \text{m}^{-2}$ to $74.8 \text{ W} \cdot \text{m}^{-2}$, respectively, at the footprint scale. At the pixel scale, the RMSEs of the revised model estimates of the H and LE were $40.9 \text{ W} \cdot \text{m}^{-2}$ and $57.5 \text{ W} \cdot \text{m}^{-2}$, respectively. The improved agreements between the estimates and the measurements indicate that the revised SEBS model is appropriate for estimating regional energy fluxes over heterogeneous oasis–desert surfaces. Furthermore, the spatial and temporal patterns of the LE in the middle reaches of the Heihe River were investigated.

Index Terms—Heterogeneous, oasis–desert, parameterization, remote sensing, surface energy fluxes.

I. INTRODUCTION

ACCURATE evapotranspiration (ET) estimates are of crucial importance in water resource management, hydrological surveys, and climate change. ET models that are based on remotely sensed data include four main categories [1].

Manuscript received February 28, 2014; revised July 28, 2014 and September 1, 2014; accepted September 5, 2014. This work was supported in part by the National Natural Science Foundation of China under Grant 91125002 and in part by the Fundamental Research Funds for the Central Universities under Grant 2012YBXS23. (Corresponding author: Shaomin Liu.)

Y. Ma is with the State Key Laboratory of Remote Sensing Science and the School of Geography, Beijing Normal University, Beijing 100875, China, and also with the Department of Geography, Handan College, Hebei 056005, China (e-mail: maayanfei@126.com).

S. Liu, F. Zhang, Z. Jia, and L. Song are with the State Key Laboratory of Remote Sensing Science and the School of Geography, Beijing Normal University, Beijing 100875, China (e-mail: smliu@bnu.edu.cn; zhangfen911006@126.com; jzz@mail.bnu.edu.cn; scauls@163.com).

J. Zhou is with the University of Electronic Science and Technology of China, Chengdu 611731, China (e-mail: jzhou233@uestc.edu.cn).

Color versions of one or more of the figures in this paper are available online at <http://ieeexplore.ieee.org>.

Digital Object Identifier 10.1109/LGRS.2014.2356652

Although most of these models perform well over homogeneous surfaces, further investigation is needed to determine whether these models accurately estimate surface energy fluxes over heterogeneous surfaces, including oases, wetlands, and deserts. In addition, the validation of turbulent heat fluxes using “point” scale measurements obtained with the Bowen ratio, lysimeter, or eddy covariance (EC) system may raise questions because of surface heterogeneity and scaling effects. Remote sensing observations provide the potential to bridge the gap between point or patch measurements and larger scale surface processes. The Multi-Scale Observation Experiment on Evapotranspiration over heterogeneous land surfaces of the Heihe Water Allied Telemetry Experimental Research (HiWATER-MUSOEXE) program provided detailed and comprehensive observations of multiscale ET and surface parameters and meteorological factors in the middle reaches of the Heihe River from May to September 2012 [2], [3]. This field campaign permitted a unique opportunity to assess the performance of ET model estimates.

The surface energy balance system (SEBS) model has been evaluated and applied to various land covers [4]–[8]. However, a broader investigation into the application of the SEBS model for arid and semiarid regions should be performed.

The purpose of this letter is to evaluate the SEBS model performance and to improve parameterization using the field measurements. Furthermore, regional energy fluxes will be estimated, and the spatial and temporal patterns of latent heat flux over heterogeneous surfaces in the middle reaches of the Heihe River will be analyzed.

II. STUDY AREA AND DATA SET

A. Study Area Description

The Zhangye oasis is located in the middle reaches of the Heihe River Basin in northwest China. The primary underlying surfaces of this area, which include oasis cropland, residential areas, wetland, sandy desert, desert steppe, and the Gobi desert, are representative of the main underlying surface types within the middle reaches of the Heihe River Basin. The first thematic experiment launched under the HiWATER campaign was the HiWATER-MUSOEXE, which was performed within two nested experimental areas [2]. The larger experimental area (LEA) covered an area of $30 \text{ km} \times 30 \text{ km}$ [see Fig. 1(a)] over oasis–desert surfaces. The kernel experimental area (KEA) covered an area of $5.5 \text{ km} \times 5.5 \text{ km}$ over oasis surfaces

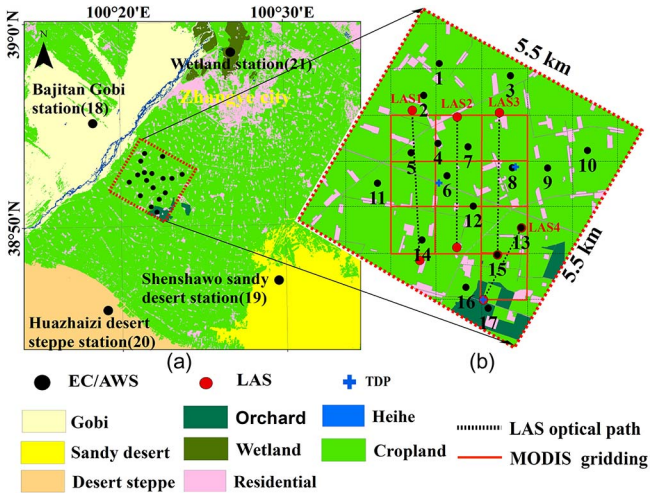


Fig. 1. Spatial locations of the 21 sites used in this study over two nested experimental areas during HiWATER-MUSOEXE.

[see Fig. 1(b)]. Moreover, in the KEA, 17 elementary sampling plots (ESPs) [including one for vegetables (site 1), one for villages (site 4), one for orchards (site 17), and fourteen for maize (sites 2, 3, 5–16)] were established according to the crop structure, shelterbelt, residential area, soil moisture, and irrigation status. In each ESP, an automatic weather station (AWS) and an EC system were installed. The 21 AWSs (four AWSs around the oasis) and 22 EC systems (two EC systems at site 15) were installed in the whole experimental areas [see Fig. 1]. In addition, four large-aperture scintillometer (LAS) systems were installed in three 3×1 and one 2×1 MODIS pixels [see the red grid in Fig. 1(b)]. Thermal dissipation sap flow probes (TDP) were installed at three sites to measure the transpiration of the shelter belt (see the blue crosses in Fig. 1).

B. Data Set

Turbulent fluxes were measured using an EC system with a sampling frequency of 10 Hz. The raw data were processed using Edire software (<http://www.geos.ed.ac.uk/abs/-research/micromet/EdiRE/>) [3], [9]. The sensible heat flux (H) and the latent heat flux (LE) from the EC system were corrected for closure using the Bowen ratio closure method. The soil heat fluxes were measured using three heat flux plates located 6 cm below ground at each site. Two plates were buried under the bare soil between two corn plants; another plate was buried under the corn plants. The surface soil heat flux, i.e., G_0 , was calculated using the “PlateCal” approach [10] based on the weighted vegetation fraction combined with the soil temperature and moisture measured above the heat plates. All micrometeorological and flux data were processed to 30-min intervals. Additional measurement and calculation details are provided in [3] and [9]. Ground measurement data (i.e., 11 ESPs in three 3×1 and one 2×1 MODIS pixels) were collected to obtain relative true values of surface energy fluxes at the pixel scale for model validation. Observed H or LE values from 11 ESPs were aggregated at the pixel scale using the area weighting method and compared with the corresponding LAS observations. However, when the relative aggregating errors are greater than a certain threshold value, the Priestley–Taylor

equation method should be used to provide relative true values of surface energy fluxes at the pixel scale by introducing retrieving land surface temperature (LST) from remote sensing. For regional estimates of the surface energy fluxes, spatial distributions of meteorological data, including air temperature (T_a), relative humidity (RH), wind speed (U), and air pressure (P) obtained from the 21 AWSs in the LEA, were interpolated using the inverse distance weighted method.

Nine Advanced Spaceborne Thermal Emission and Reflection Radiometer (ASTER, <http://global.jaxa.jp/>) images were acquired from June to September 2012. The LST was retrieved from the thermal infrared bands whose spatial resolution was 90 m, using the split-window algorithm. Cloud-free images were subsequently used to calculate the normalized differential vegetation index, fractional vegetation cover, leaf area index, and albedo. The land use data were generated using the supervised classification method.

III. METHODOLOGY

A. SEBS Model

The SEBS model was used to estimate the H, LE, net radiation, (R_n), and G_0 based on a surface energy balance equation using remote sensing data and meteorological information; H can be determined from iterating a series of nonlinear equations. R_n is estimated from radiation balance equation by combining remote sensing data, e.g., LST and albedo. Further details on the SEBS model are presented in [4]. To evaluate the performance of the SEBS model, four evaluation indexes were utilized, i.e., the mean bias error (MBE), the mean absolute percent error (MAPE), the root-mean-square error (RMSE), and the correlation coefficient (R).

An underestimation of H using the SEBS model has been reported by [6] and [7]. To evaluate the original SEBS performance for each land cover class in these arid and semiarid regions, H, LE, R_n , and G_0 measurements from the 21 sites were compared with the SEBS model estimates for the land covers of the Gobi desert, sandy desert, desert steppe, residential areas, agricultural cropland (maize and vegetable), orchard, and wetland (see the left column in Fig. 2). The accuracy assessment is listed in Table I. The results indicate that R_n had higher estimation accuracy, with an MAPE of 2.5% and an RMSE of $29.0 \text{ W} \cdot \text{m}^{-2}$ (see Table I). The SEBS model underestimated H, particularly for high H ranges, compared with EC measurements (see Fig. 2). The gray-shaded area represents the greatest underestimates of H, which implies that model underestimation occurs particularly for bare soil and sparse vegetation land cover and partly for agricultural crops (see Fig. 2). Consequently, a pronounced overestimation of the latent flux was observed; G_0 of the SEBS model estimating was relatively discretely scattered (see Fig. 2). On the basis of this analysis, it is crucial to optimize the parameterization scheme in the SEBS model by using observational data to accurately estimate regional surface energy fluxes over heterogeneous oasis–desert landscapes in arid and semiarid regions [11].

The SEBS model includes many land surface physical parameters. Some of them are very uncertain because of the effect of heterogeneous surface and scaling effects [12]. van der Kwast *et al.* [13] suggested that the sensitivity of the

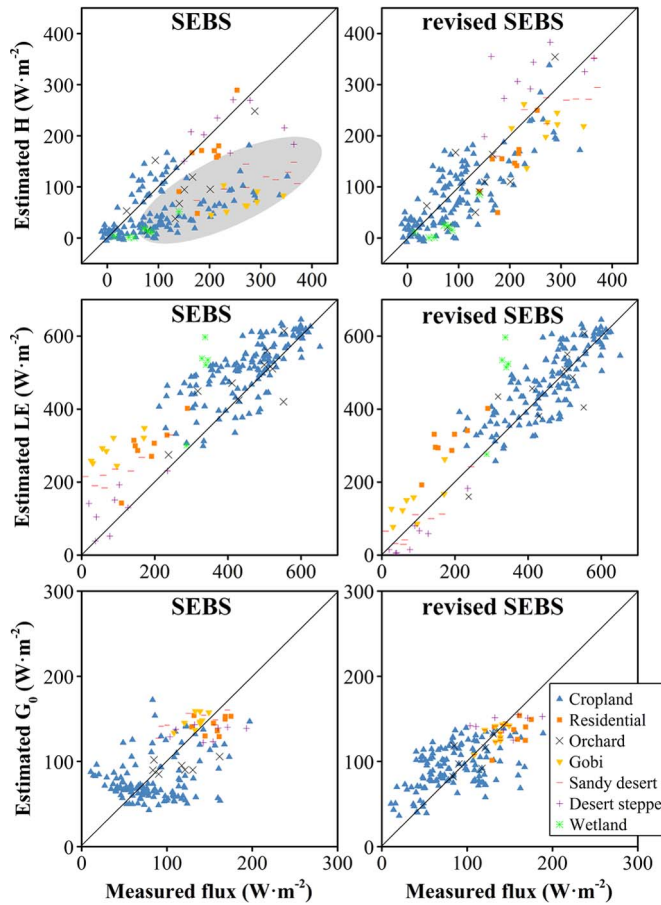


Fig. 2. Instantaneous H, LE, and G_0 ($\text{W} \cdot \text{m}^{-2}$) values estimated using the (left column) SEBS model and the (right column) revised SEBS model compared with the EC measurements at nine ASTER overpass times.

TABLE I
COMPARISON OF SURFACE ENERGY FLUXES ESTIMATED USING THE SEBS MODEL AND THE REVISED SEBS MODEL

Model	Flux	MBE($\text{W} \cdot \text{m}^{-2}$)	MAPE (%)	RMSE($\text{W} \cdot \text{m}^{-2}$)	R(-)
SEBS	R_n	-6.5	2.5	29.0	0.92
	H	-61.7	56.5	97.2	0.63
	LE	68.0	20.6	102.9	0.88
	G_0	-2.8	30.9	37.0	0.56
Revised SEBS	H	-15.8	34.7	56.9	0.84
	LE	23.0	14.9	74.8	0.90
	G_0	7.9	28.9	33.6	0.64

SEBS model's parameters was determined by the LST, surface roughness length for momentum, i.e., z_{0m} , wind speed, and shortwave incoming radiation. Subsequently, we analyzed the sensitivity of the model parameters using the random-sampling high-dimensional model representation method [14]. We found that R_n , z_{0m} and surface roughness length for heat transfer, i.e., (z_{0h}), G_0 , and LST are the most important factors that affect the surface energy fluxes estimated by the SEBS model. The current LST retrieval precision is approximately 2 K, which leaves limited room for improvement, and the precision of the estimated R_n agreed well with the measurements (see Table I). Therefore, the G_0 , z_{0m} , and z_{0h} parameterization schemes were optimized to improve the model precision.

B. Development of the Surface Soil Heat Flux Parameterization

It is difficult to accurately estimate G_0 at the regional scale. In the SEBS model, G_0 is estimated as a fraction of R_n , i.e., Γ [4]. The original parameterization of soil heat flux produces low accuracy of estimated G_0 at regional scale (see Fig. 2), which could affect estimation of LE.

Tanguy *et al.* have recently proposed a parameterization of G_0 as a function of the evaporative fraction and noted that the physical rationale (Γ) has relations with soil temperature and soil moisture availability [15]. In this letter, based on G_0 is expected to increase with the soil temperature gradient, which is a decreasing function of soil moisture availability, we developed another formula for Γ based on the temperature-vegetation dryness index (TVDI), i.e.,

$$\Gamma = [\Gamma_c + (\Gamma_s - \Gamma_c) \times \text{TVDI}] \quad (1)$$

where Γ_s and Γ_c are 0.315 for bare soil and 0.05 for full vegetation canopy, respectively, according to Su [4].

C. Revision of the Surface Roughness Length

Previous studies have established several relational expressions between z_{0m} and surface elements (such as the canopy height and the vegetation index) [16]. Experiments have shown that z_{0m} is affected by the height, structure, spatial distribution of surface roughness elements, and a combination of aerodynamic and thermodynamic factors [17]. In this letter, based on the work of Zhang *et al.* [17], a natural logarithm model for converting the equivalent geometric roughness within the fetch to surface roughness length for momentum transfer was built and presented in the following:

$$\ln(z_{0m}) = \xi \ln(\eta) + \xi_0 \quad (2)$$

$$\eta = \frac{\sum_x \sum_{y=0}^{200} \text{HC}(x, y) \left(\frac{1}{D(x, y)}\right)^{2.5} \left(\frac{|\Delta \text{LST}(x, y)|}{\text{LST}}\right)^{0.5}}{\sum_x \sum_{y=0}^{200} \left(\frac{1}{D(x, y)}\right)^{2.5} \left(\frac{|\Delta \text{LST}(x, y)|}{\text{LST}}\right)^{0.5}} \quad (3)$$

where η is the equivalent geometric roughness for a specific pixel, ξ and ξ_0 are the model transformation factors, x and y are the pixel location, HC is the canopy height at the pixel, $D(x, y)$ is the distance between a point and the measured point, and $\Delta \text{LST}(x, y)$ is the difference between the air temperature at the reference height and the LST. Furthermore, the fanlike area Ω was mapped using an arc and two straight border lines, which form 30° fanlike arcs along the windward side. The length along the two straight border lines in the y -direction is "200." In our study, the relationship between z_{0m} and η was calibrated during HiWATER-MUSOEXE with a minimal RMSE criterion. The calibrated model transformation factors (i.e., ξ and ξ_0) were equal to 0.39 and -0.76 , respectively. Moreover, an R of 0.89 was determined for our experiment, which included residential areas, corn crops, orchard, sandy desert, the Gobi desert, and wetland surfaces.

The difference between z_{0m} and z_{0h} can be described as an excess resistance parameter, i.e., kB^{-1} . The SEBS model is highly sensitive to the z_{0h} or kB^{-1} parameter, rendering marked differences in heat flux estimates under different

treatments of roughness length for heat transfer [18]. In this letter, we evaluated the z_{0h} or kB^{-1} parameterization schemes using tower-based measurements at the sites, and the kB^{-1} parameterization schemes of Yang *et al.* [19], Kanda *et al.* [20], and Bosveld *et al.* [21] were used for underlying surfaces of bare soil, residential areas, and highly dense vegetation, respectively. The kB^{-1} for sparse vegetation in the region was the same as the parameterization defined by Su [4].

D. Footprint Model

A Eulerian analytical expression was adopted to obtain the flux footprint of the EC system [22]. We then set the flux contribution of the chosen total source area at 95% for every 30 min [9]. In this letter, the footprint-integrated H and LE at the 90-m ASTER pixel were compared with EC measurement.

IV. RESULTS AND DISCUSSION

A. Revised SEBS Model Validation at the Footprint Scale

In this letter, the footprint-integrated H and LE [1] at the 90-m ASTER pixels were compared with the EC measurements from 21 sites (see Table I and Fig. 2). The plots (see the right column in Fig. 2) demonstrate good correspondence between the instantaneous observations and model outputs at different land use/cover sites. The RMSE of H decreased from $97.2 \text{ W} \cdot \text{m}^{-2}$ to $56.9 \text{ W} \cdot \text{m}^{-2}$ (see Table I). Moreover, the MAPE decreased from 56.5% to 34.7%, R increased from 0.63 to 0.84, and the RMSE of LE decreased from $102.9 \text{ W} \cdot \text{m}^{-2}$ to $74.8 \text{ W} \cdot \text{m}^{-2}$. In addition, the MAPE decreased from 20.6% to 14.9%, and R increased from 0.88 to 0.90. Because a majority of H was small and approximately $0\text{--}100 \text{ W} \cdot \text{m}^{-2}$ in the oasis during July and August, it exhibited relatively large fluctuations and likely contained large uncertainties. Therefore, the MAPE of H was greater than that of LE. The new formula for G_0 [see (1)] agreed better with the measurements than the G_0 parameterization for the SEBS model (see Fig. 2); R was 0.64, the MAPE was 28.9%, the MBE was $7.9 \text{ W} \cdot \text{m}^{-2}$, and the RMSE was $33.6 \text{ W} \cdot \text{m}^{-2}$ for the new scheme (see Table I). The reported results here indicated that the revised SEBS model performed very well over the heterogeneous oasis–desert surfaces.

B. Revised SEBS Model Validation at the Pixel Scale

We validated the H and LE estimates from the revised SEBS model at three 3×1 and one 2×1 MODIS pixel scales in the center of the KEA. The results indicate that the instantaneous H was in better agreement with the pixel scale values; R was 0.87, the regression slope was 0.80, and the RMSE was $40.9 \text{ W} \cdot \text{m}^{-2}$ (see Fig. 3). Moreover, the instantaneous LE was consistent with the pixel scale value; R was 0.85, the regression slope was 1.07, and the RMSE was $57.5 \text{ W} \cdot \text{m}^{-2}$. This further proves that the estimation accuracy of the revised SEBS model was markedly improved by optimization.

C. Spatial and Temporal Patterns of LE

The spatial and temporal patterns of the instantaneous satellite-based LE at a 90-m resolution over the study area

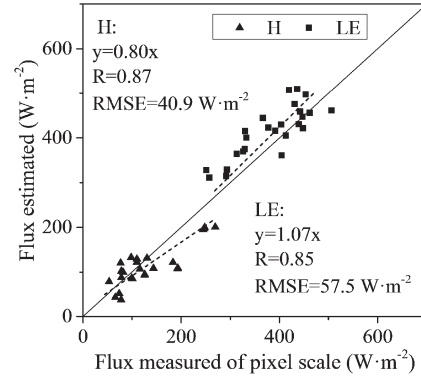


Fig. 3. Instantaneous satellite-based H and LE values using the revised SEBS model compared with the relative true values of pixel scale.

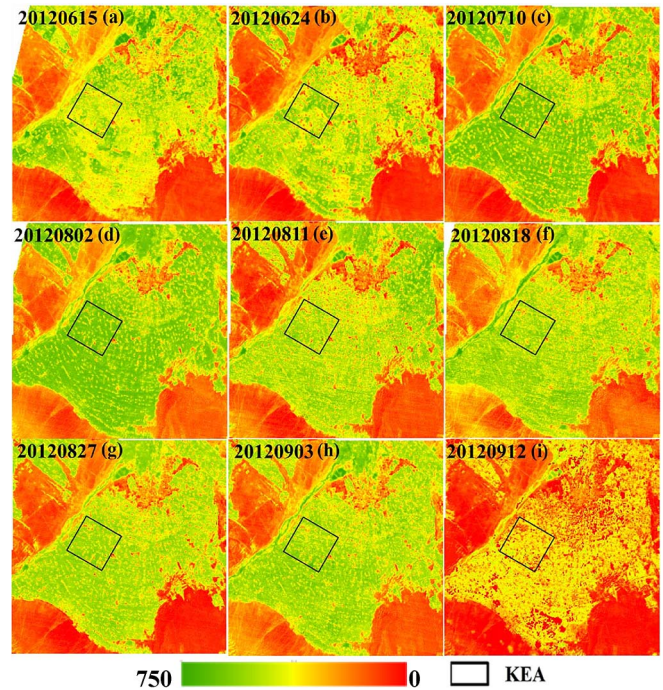


Fig. 4. Maps of the instantaneous satellite-based LE ($\text{W} \cdot \text{m}^{-2}$) at ASTER overpass times (approximately 12:15 GMT+8). The KEA of each map of the instantaneous LE is marked by a black square.

are shown in Fig. 4. The instantaneous LE in the LEA exhibited high spatial variability that was attributed to the spatial heterogeneity of the soil moisture, vegetation, and meteorological conditions. The statistical results of the land use/cover indicate that the wetland LE was the largest, i.e., greater than $500 \text{ W} \cdot \text{m}^{-2}$ in July and August. Although the precipitation was sparse, irrigation water was relatively abundant during the growing season (four to five flood irrigations per season). Therefore, the oasis cropland (i.e., the maize and vegetable land cover types) and orchard had higher LE values that ranged from 400 to $500 \text{ W} \cdot \text{m}^{-2}$. However, in the areas surrounding the oasis, such as the sandy desert, the Gobi desert, and desert steppe, the LE was generally less than $250 \text{ W} \cdot \text{m}^{-2}$ in July and August because of sparse precipitation and no irrigation. Additionally, in residential areas, such as Zhangye city, villages, and roads, the LE was less than $300 \text{ W} \cdot \text{m}^{-2}$. The LE spatial patterns captured seasonal changes during the growing season, too. The date of closing of crop was approximately July 10. The heterogeneity of oasis farmland LE was relatively high before the full

crop, but then, the inhomogeneity decreased considerably. The irrigation events had a greater effect on increasing oasis internal heterogeneity, except for the villages and roads. For example, on June 24, the soil moisture measured at a depth of 0.04 m at sites 3, 9, and 10, which were irrigated, was approximately 37% compared with approximately 22% at the nonirrigated sites. The average LE of sites 3, 9, and 10 was $549.7 \text{ W} \cdot \text{m}^{-2}$ compared with $453.2 \text{ W} \cdot \text{m}^{-2}$ for the nonirrigated sites. The ET map on June 24 further confirms the water management practices, particularly the irrigated areas at the northeast edge of the KEA [see Fig. 4(b)]. In early September at the end of the growing season, most of the maize had withered from frost, which was accompanied by a decrease in the ET of the entire oasis [see Fig. 4(i)]. In the absence of irrigation, the influence of precipitation in the surrounding sandy desert, desert steppe, and the Gobi desert was evident in the LE values. For example, there was 5–10 mm of rainfall before August 2 or August 11, and the LE increased significantly in the surrounding sandy desert, desert steppe, and the Gobi desert [see Fig. 4(d) and (f)]. The LE for the primary land cover classes suggested that the LE was higher in July and August and lower in June and September. This finding can be explained by the relative increase in precipitation and phenology responses in July and August compared with June and September.

V. CONCLUSION

In this letter, we have optimized the z_{0m} , z_{0h} or kB^{-1} , and G_0 approaches and estimated the regional surface energy fluxes over heterogeneous oasis-desert surfaces during HiWATER-MUSOEXE. The satellite-based instantaneous H and LE values were validated using EC measurements at the footprint scale and the relative true values at the pixel scale. The estimated RMSEs of the LE were $74.8 \text{ W} \cdot \text{m}^{-2}$ and $57.5 \text{ W} \cdot \text{m}^{-2}$ at the footprint and pixel scales, respectively, using the revised SEBS model, which are improved compared with previous studies [11], [23]. The LE varied considerably over the LEA and decreased from the internal oasis to the surrounding sandy desert, desert steppe, and the Gobi desert. The LE values were higher in July and August and lower in June and September. The LE values of wetlands, oasis croplands, orchards, residential areas, desert steppe, the Gobi desert, and sandy desert were reduced in succession. In addition, irrigation and precipitation events impacted the spatiotemporal patterns of LE over the oasis-desert landscape. The results from this study suggest that the revised SEBS model has potential for producing reliable ET estimates over oasis-desert landscapes, which will benefit water resource management in river basins and will also aid in irrigation decisions.

ACKNOWLEDGMENT

The authors would like to thank all the scientists, engineers, and students who participated in the HiWATER-MUSOEXE.

REFERENCES

- [1] Z. Z. Jia, S. M. Liu, Z. W. Xu, Y. J. Chen, and M. J. Zhu, "Validation of remotely sensed evapotranspiration over the Hai River Basin, China," *J. Geophys. Res.*, vol. 117, D13113, Jul. 2012. DOI: 10.1029/2011JD017037.
- [2] X. Li *et al.*, "Heihe watershed allied telemetry experimental research (HiWATER): Scientific objectives and experimental design," *Bull. Amer. Meteorol. Soc.*, vol. 94, no. 8, pp. 1145–1160, Aug. 2013.
- [3] Z. W. Xu *et al.*, "Intercomparison of surface energy flux measurement systems used during the HiWATER-MUSOEXE," *J. Geophys. Res.*, vol. 118, no. 23, pp. 13140–13157, Dec. 2013.
- [4] Z. Su, "The surface energy balance system (SEBS) for estimation of turbulent heat fluxes," *Hydrol. Earth Syst. Sci.*, vol. 6, no. 1, pp. 85–99, 2002.
- [5] L. Jia *et al.*, "Estimation of sensible heat flux using the Surface Energy Balance System (SEBS) and ATSR measurements," *Phys. Chem. Earth, Part A/B/C*, vol. 28, no. 1–3, pp. 75–88, 2003.
- [6] J. Chirouze *et al.*, "Intercomparison of four remote-sensing-based energy balance methods to retrieve surface evapotranspiration and water stress of irrigated fields in semi-arid climate," *Hydrol. Earth Syst. Sci.*, vol. 18, no. 3, pp. 1165–1188, Mar. 2014.
- [7] M. F. McCabe and E. F. Wood, "Scale influences on the remote estimation of evapotranspiration using multiple satellite sensors," *Hydrol. Process.*, vol. 105, no. 4, pp. 271–285, Dec. 2006.
- [8] Y.-A. Liou and S. K. Kar, "Evapotranspiration estimation with remote sensing and various surface energy balance algorithms—A review," *Energies*, vol. 7, no. 5, pp. 2821–2849, Apr. 2014.
- [9] S. M. Liu *et al.*, "A comparison of eddy-covariance and large aperture scintillometer measurements with respect to the energy balance closure problem," *Hydrol. Earth Syst. Sci.*, vol. 15, no. 4, pp. 1291–1306, Apr. 2011.
- [10] C. Liebenthal, B. Huwe, and T. Foken, "Sensitivity analysis for two ground heat flux calculation approaches," *Agr. Forest Meteorol.*, vol. 132, no. 3/4, pp. 253–262, Oct. 2005.
- [11] W. Ma *et al.*, "Estimating surface fluxes over middle and upper streams of the Heihe River Basin with ASTER imagery," *Hydrol. Earth Syst. Sci.*, vol. 15, no. 5, pp. 1403–1413, May 2011.
- [12] Y. A. Liou, E. J. Kim, and A. W. England, "Radiobrightness of prairie soil and grassland during dry-down simulations," *Radio Sci.*, vol. 33, no. 2, pp. 259–265, Mar./Apr. 1998.
- [13] J. van der Kwast *et al.*, "Evaluation of the Surface Energy Balance System (SEBS) applied to ASTER imagery with flux-measurements at the SPARC 2004 site (Barrax, Spain)," *Hydrol. Earth Syst. Sci.*, vol. 13, no. 7, pp. 1337–1347, Jul. 2009.
- [14] T. Ziehn and A. S. Tomlin, "GUI-HDMR—A software tool for global sensitivity analysis of complex models," *Environ. Model. Softw.*, vol. 24, no. 7, pp. 775–785, Jul. 2009.
- [15] M. Tanguy *et al.*, "A new parameterization scheme of ground heat flux for land surface flux retrieval from remote sensing information," *J. Hydrol.*, vol. 454/455, pp. 113–122, Aug. 2012.
- [16] W. Bastiaanssen, "Regionalization of surface flux densities and moisture indicators in composite terrain," Ph.D. dissertation, Wageningen Agriculture Univ., Wageningen, The Netherlands, 1995.
- [17] R. H. Zhang, F. Wang, C. Y. Zhu, X. M. Sun, and Z. L. Zhu, "The retrieval of two-dimensional distribution of the Earth's surface aerodynamic roughness using SAR image and TM thermal infrared image," *Sci. China Ser. D, Earth Sci.*, vol. 47, no. 12, pp. 1134–1146, Dec. 2004.
- [18] Y. C. Gao and D. Long, "Intercomparison of remote sensing-based models for estimation of evapotranspiration and accuracy assessment based on SWAT," *Hydrol. Process.*, vol. 22, no. 25, pp. 4850–4869, Dec. 2008.
- [19] K. Yang, T. Koike, H. Fujii, K. Tamagawa, and N. Hirose, "Improvement of surface flux parameterizations with a turbulence-related length," *Q. J. R. Meteorol. Soc.*, vol. 128, no. 584, pp. 2073–2087, Jul. 2002.
- [20] M. Kanda, M. Kanega, T. Kawai, R. Moriwaki, and H. Sugawara, "Roughness lengths for momentum and heat derived from outdoor urban scale models," *J. Appl. Meteorol. Climatol.*, vol. 46, no. 7, pp. 1067–1079, Jul. 2007.
- [21] F. C. Bosveld, A. A. M. Holtslag, and B. J. J. M. Van Den Hurk, "Interpretation of crown radiation temperatures of a dense Douglas fir forest with similarity theory," *Bound.-Lay. Meteorol.*, vol. 92, no. 3, pp. 429–451, Sep. 1999.
- [22] R. Kormann and F. X. Meixner, "An analytical footprint model for non-neutral stratification," *Bound.-Lay. Meteorol.*, vol. 99, no. 2, pp. 207–224, May 2001.
- [23] X. M. Li, L. Lu, W. F. Yang, and G. D. Cheng, "Estimation of evapotranspiration in an arid region by remote sensing—A case study in the middle reaches of the Heihe River Basin," *Int. J. Appl. Earth Observ. Geoinf.*, vol. 17, pp. 85–93, Jul. 2012.